Broadband Point Measurement of Transient Magnetic Interference in Substations With Magnetoresistive Sensors

Qi Huang[1], Xiaohua Wang[1], Wei Zhen[2], and Philip W. T. Pong[3]

[1]School of Energy Science and Engineering, University of Electronic Science and Technology of China,
Chengdu 611731, China
[2]Sichuan Electric Power Test and Research Institute, Chengdu 610072, China
[3]Department of Electrical and Electronic Engineering, the University of Hong Kong, Hong Kong

Electromagnetic interference (EMI) in substations can be an obstacle for the development of the Smart Grid. This challenge is particularly critical since more and more secondary systems are transferred from control rooms to switching yards in modern power systems. Thus, it is important to develop a tool that can properly characterize and evaluate the EMI level. This paper introduces a novel broadband point measurement technology for evaluating the effect of transient magnetic field (TMF) on secondary systems in substations. The received disturbance level is defined for the victim circuit and the evaluation approach is proposed. The effect of sensor size on the measurement of TMF is explained and illustrated with numerical simulation, indicating the importance of point measurement. The designed measurement system was tested and the TMF caused by charging traveling wave in a 110-kV substation was characterized. Our results show that the TMF may produce significant effect on the secondary systems in a substation, and thus it is important to have the capability to evaluate the interference level.

Index Terms—**Broadband point measurement, magnetoresistive (MR) sensor, substation, transient magnetic field (TMF).**

I. INTRODUCTION

WITH the development of the Smart Grid, electronic devices, such as solid-state protective relays, microprocessor-based control units are increasingly used in power systems for various purposes [1], [2]. In particular, certain smart electronics devices traditionally deployed in control rooms are now installed close to the high-voltage equipment in the switching yards [3]. These make the measurement and evaluation of transient electromagnetic (EM) fields produced by switching or lightning become more and more important to ensure electromagnetic interference (EMI) compatibility.

Under transient conditions, the secondary systems installed in switching yards endure atrocious EMI environment composing of transient magnetic field (TMF) and transient electric field (TEF). This paper focuses on the measurement and evaluation of TMF for two reasons. First, it is more difficult to shield magnetic field than electric field. Since the standards for the Smart Grid are still far from completion [4], many onsite cabinets in the substations, traditionally located in control room but now in switching yard, are not properly shielded against TMF. Second, overcurrent is more of a menace than overvoltage [5] because overvoltage is generally well protected in substations. Hence, the disturbances caused by TMF can be much more disastrous than that caused by TEF.

The measurement of EMI is a difficult task because EMI generally appears in very wide frequency band [3]–[6]. Commercially available EMI meters generally can only measure the interference level without the functionality of high-frequency waveform analysis. To identify the actual power system faults, it is necessary to obtain the waveform of the transient interference for analysis. A search coil can be used to measure

high-frequency EMI [7]; however, this solution does not work well for low-frequency EMI and is not easy for miniaturization to perform point measurement. As such, it is imperative to find a solution which can realize broadband point measurement of EMI.

In addition to the interference level of TMF, it is necessary to evaluate the effect of the TMF on the victim circuits which are typically the secondary system circuits [8], such as communication or control devices used in substations. An ideal instrumentation device for measuring TMF in substations should possess the following capabilities: 1) measurement of TMF with high-spatial resolution; 2) sufficient bandwidth and dynamic range; and 3) correlate the EMI to power system events for long-term quantitative evaluation of EMI.

In this paper, the TMF measurement system was developed based on magnetoresistive (MR) sensors. MR sensors [9], with their favorable characteristics, such as high sensitivity, compact-in-size, large temperature range, broad bandwidth (dc-~MHz), and easily integratable with microelectromechanical system (MEMS) for three-axis point measurement of vector magnetic field, can be used to evaluate the spatial TMF. There are already many successful applications of MR sensors found in the Smart Grid [10], [11].

The rest of the paper is organized as follows. In Section II, the measurement system design is presented and the approach for evaluating the effect of TMF on the secondary circuit is proposed. The numerical and experimental results are discussed in Section III, and Section IV presents the conclusion.

II. EVALUATION APPROACH OF SPATIAL TMF AND EFFECT OF SENSOR SIZE

A. Evaluation Approach of Spatial TMF

The EMI problem involves the source, the propagation route, and the victim circuit. The impact of TMF is dependent on many parameters such as peak level, average level, total energy, frequency, modulation, and so on. The induced voltage
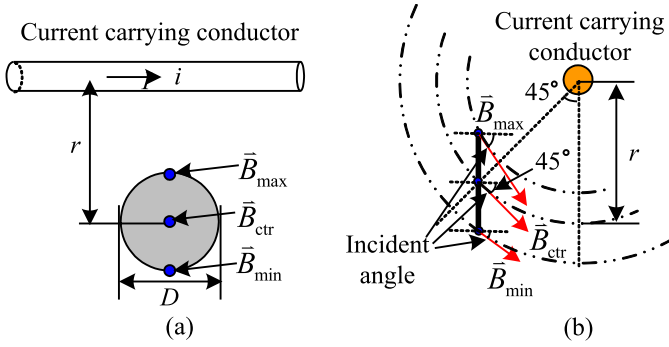
Fig. 1.   Effect of sensor size in measurement of magnetic field. (a) Sensor vertically below the conductor. (b) Sensor below conductor at 45° direction.
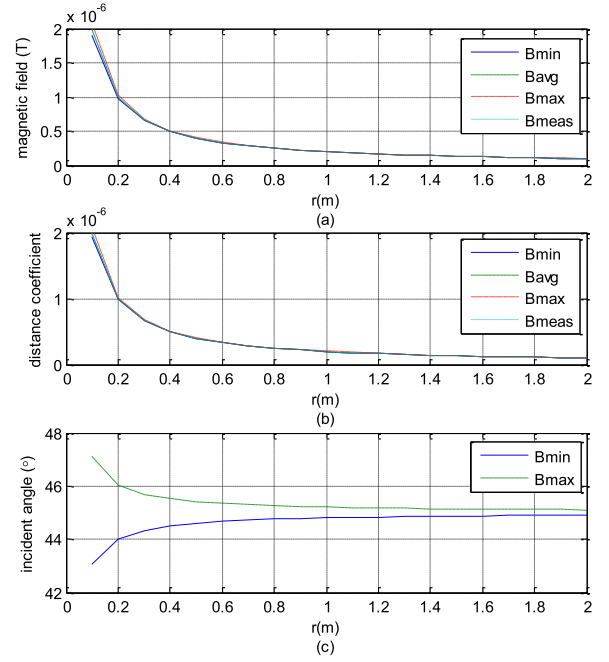

Fig. 2.   Effect of sensor size in measurement of magnetic field. (a) Magnetic field at different points when sensor is vertically below the conductor. (b) Magnetic field at different points when sensor is below conductor at 45° direction. (c) Incident angle of magnetic field at the farthest point and the closest point.

is proportional to the derivative of the flux, and it is defined as the received disturbance level at the victim circuit

$$\varepsilon(t) = \frac{d\phi(t)}{dt} = \vec{A} \cdot \frac{d\vec{B}(t)}{dt} \qquad (1)$$

where $\vec{A}$ is the area of the victim circuit projected onto the direction of the local incident magnetic field, $\phi(t)$ is the flux, and $\vec{B}(t)$ is the local TMF vector. The induced voltage is the most important parameter in evaluating the effect of TMF on the secondary systems in substations. The response of the victim circuit $v(t)$ to the disturbance can be evaluated with the following equation:

$$v(t) = \mathrm{A}L^{-1}(s\hat{g}(s)B(s)) \qquad (2)$$

where $B(s)$ is the Laplace transform of measured magnetic field vector $\vec{B}(t)$, $\hat{g}(s)$ is the transfer function between induced voltage $\varepsilon(t)$ and output $v(t)$, $L^{-1}()$ is inverse Laplace transform, and A is the area of the victim circuit perpendicular to the direction of $\vec{B}(t)$.

From (1), the effect of the TMF on the victim circuit can be directly evaluated by calculating the derivative of $\vec{B}(t)$. Nevertheless, in practice, it is not so convenient to obtain the derivative of TMF due to the noise and analog–digital quantizing error. For engineering application, one can first perform the Fourier transform of the measured magnetic field waveform, and then find the frequency components and their effects by computing $|\omega B(\omega)|$

$$\varepsilon = \vec{A} \cdot \sum_{\omega} \left| \omega \vec{B}(\omega) \right| \qquad (3)$$

where ω is the angular frequency, $\vec{B}(\omega)$ is the magnetic flux density at frequency ω.

B. Effect of Sensor Size

To demonstrate the importance of point measurement, numerical simulations are performed to illustrate the effect of the area of the sensor head on the measurement accuracy.

Suppose a circular sensor with a diameter of D is placed in the magnetic field produced by a current carrying conductor, as shown in Fig. 1. In Fig. 1(a), the sensor is placed vertically below the conductor; in Fig. 1(b), the sensor is moved to 45° direction while the distance between the center of the sensor head and the current carrying conductor r remains unchanged. The direction of current flow is perpendicular to the paper plane in Fig. 1(b). According to Biot–Savart law, the magnetic

field generated at the point with a distance r from a conductor carrying current i should be

$$B = \frac{\mu_0 i}{2\pi r} \qquad (4)$$

where μ_0 is the permeability constant ($4\pi \times 10^{-7}$ H · m^{-1}). Numerical simulation was carried out based on a magnetic search-coil sensor with $D = 1$ cm. The changes of the magnetic field vectors $\vec{B}_{ctr}$ (the magnetic field at the center point of the sensor head), $\vec{B}_{meas}$ (the average magnetic field over the sensor circular area which is the signal measured by the sensor in practice), $\vec{B}_{min}$ (the magnetic field at the farthest point of the sensor head), and $\vec{B}_{max}$ (the magnetic field at the nearest point of the sensor head) with the distance r are simulated in Fig. 2. In both cases, the magnitude of $\vec{B}_{meas}$ agrees with that of $\vec{B}_{ctr}$ very well, as shown in Fig. 2(a) and (b), respectively. However, noticeable discrepancy between the incident angles of $\vec{B}_{min}$ and $\vec{B}_{max}$ at different points on the sensor plane can be observed from Fig. 2(c). Such discrepancy is dependent on the sensor size, particularly when r is small (i.e., close to the field source). The smaller the sensor, the smaller the discrepancy. When $r = 1$ m and $D = 1$ cm, the discrepancy of the incident angle is 0.4052°. As D reduces to 3 mm, the discrepancy diminishes to 0.1216°. Thus, $\vec{B}_{meas}$ agrees with $\vec{B}_{ctr}$ more as D reduces. In order for the sensor measurement $\vec{B}_{meas}$ to truly reflect the actual magnetic field at the point (i.e., $\vec{B}_{ctr}$), the sensor size should be minimized so that $\vec{B}_{min}$ and $\vec{B}_{max}$ are as close to each other as possible. As such, point measurement (i.e., small sensor size) is critical for obtaining accurate measurement of the TMF with high-spatial resolution. Three-axis MR sensors are a promising candidate for achieving this goal because of their compact-in-size. In addition, a commercially available three-
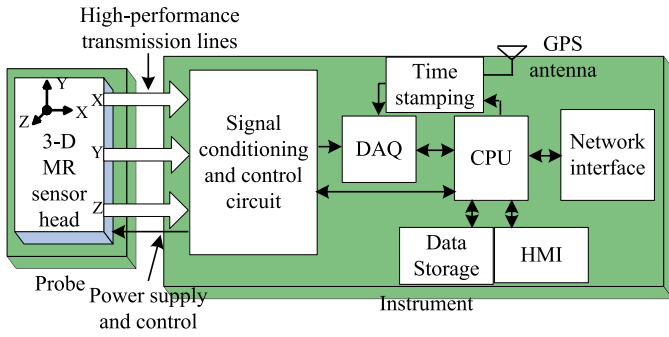
Fig. 3. System architecture of TMF point measurement system.

axis MR sensor can be fabricated into a MEMS fluxgate with a very small size (<3 mm or even less) [12] and have a dynamic range from 120 μG to 6 G. All these characteristics are favorable for designing a point measurement system of spatial TMF in substations, which requires broad frequency band (e.g., EMI caused by dc, power-frequency, or high-frequency transient) and large dynamic range (e.g., current might be tens of times of that under normal conditions).

III. DESIGN OF POINT MEASUREMENT SYSTEM AND APPLICATION TESTING

A. Design and Implementation of the Point Measurement System

Fig. 3 shows the system architecture of the measurement system. A three-axis MR sensor (HMC1043 with a packaged size of 3 × 3 × 1.5 mm) installed on a small printed circuit board serves as the probe for measuring TMF. In order not to affect the spatial distribution of the magnetic field to be measured, the ancillary circuits are assembled as another module, leaving only the MR sensor head alone on the probe. The measured weak signals are transmitted to the instrument by differential transmission in a high performance, well-shielded, and high-frequency transmission line. The signal conditioning circuits filter and amplify the received signals before data acquisition. Data storage, network interface, and human–machine interface are properly designed for convenient use in field. The signal processing and analysis algorithms are implemented on the central processing unit. Currently, GPS is widely used in power grids to perform synchronous phasor measurement [13]. A GPS antenna is installed with this system to provide time-stamped data in order to facilitate correlating the EMI to the timing of the power system outages and finding the sources of the interferences.

The whole system has a bandwidth from dc to 5 MHz, covering most transient EMI phenomena in substations, and a measurement range of $\pm$6 G (with resolution 0.02 G). Experimental characterization shows that the developed system exhibits good linearity (>99.7%) and relatively small error (>3%), as shown in Fig. 4. In the characterization experiment, the magnetic field reference is generated by driving a Helmholtz coil using a current generator. The results shown in Fig. 4 are measured at 50 Hz.

A test was carried out to investigate the system performance in measuring TMF. A standard lightning surge generator (SG-5009G) is connected to a standard magnetic field test equipment compliant with IEC 61000-4-9 [14]. The current
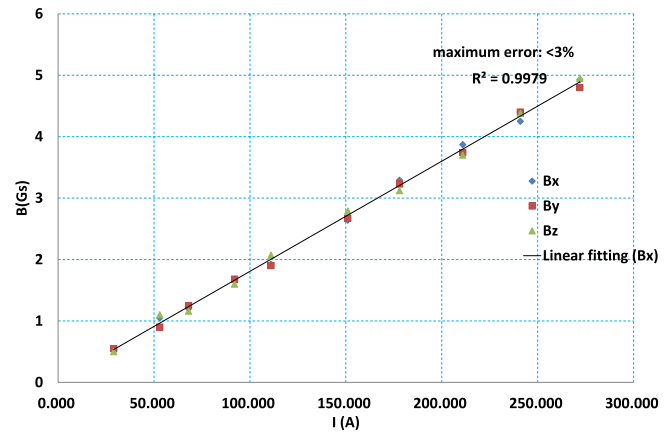

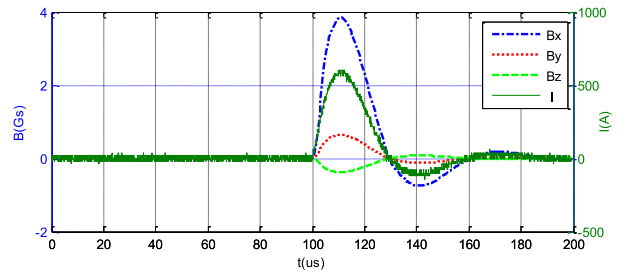Fig. 4. Evaluation of linearity and measuring error.

Fig. 5. Current pulse waveform and the resulted magnetic field measured by the developed system.
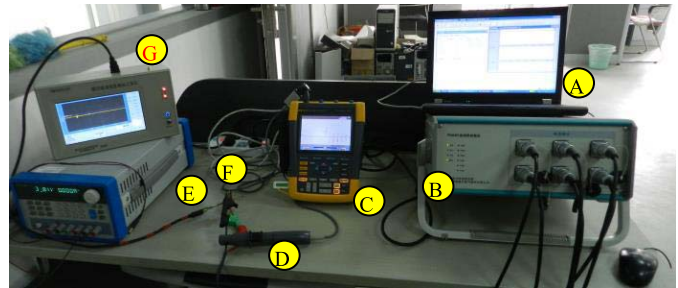

Fig. 6. Experimental setup. A: Computer. B: Traveling wave generator. C: Oscilloscope for displaying the measured current. D: Current probe. E: TMF measurement system. F: Solenoid. G: Oscilloscope for displaying the measured magnetic field.

waveform was observed by an oscilloscope while the magnetic field waveform was measured by the developed system in this paper. The results are shown in Fig. 5. It is shown that current waveform's rising time (6.65 μs) and duration time (17.4 μs) can be well followed by that of the magnetic field waveform (6.76 and 18.1 μs, respectively). Both waveforms fall in the range of the standard, i.e., 6.4 μs $\pm$ 30% and 16 μs $\pm$ 30%.

B. Experimental Setup

A traveling wave was simulated and amplified to produce transient current and TMF. The developed system was then used to measure the generated TMF. The experimental setup is shown in Fig. 6. A charging operation of a transmission line is simulated with Power System Computer Aided Design(PSCAD) software [15]. The simulated output is connected to a power amplifier (denoted as traveling wave generator in the figure) to generate up to 10 A transient current. The amplified current is connected to a small solenoid to
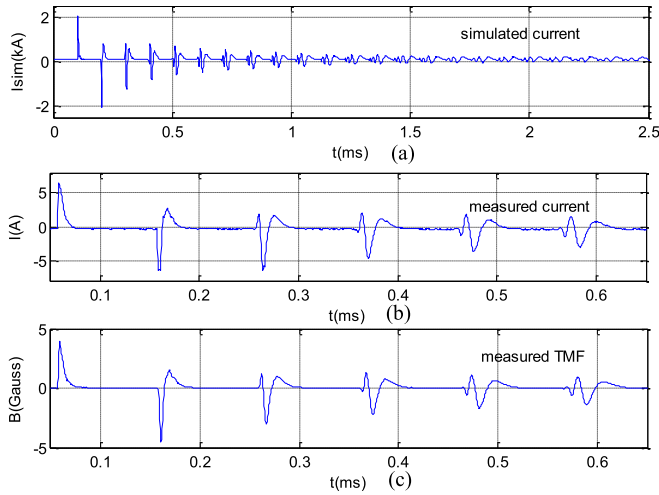
Fig. 7. Measurement results with magnetic field generated by a simulated traveling wave current passing through a power amplifier. (a) Simulated travelling current. (b) Output current measured by a current probe. (c) Magnetic field measured by the developed system.
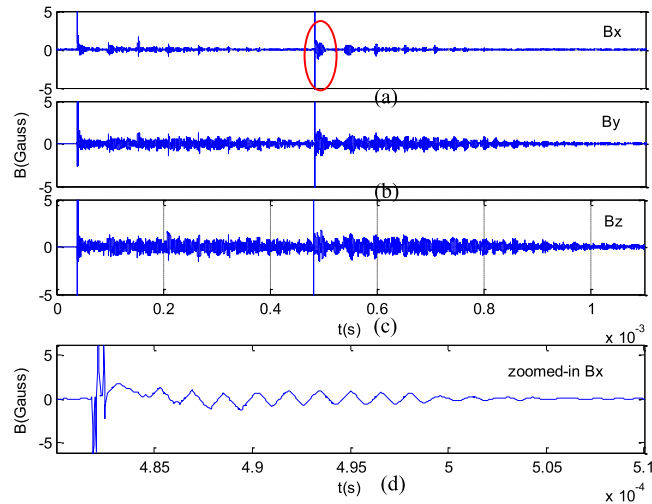

Fig. 8. Measured TMF components in the (a) x-axis, (b) y-axis, and (c) z-axis during charging busbar in a 110-kV substation. (d) Zoomed-in view of the highlighted waveform in (a).
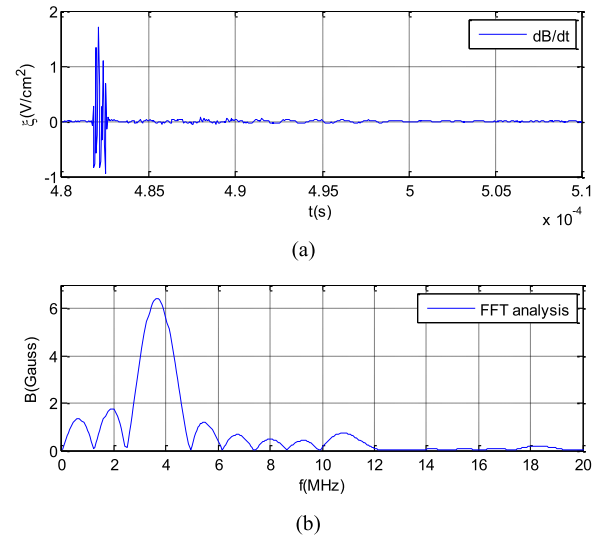

Fig. 9. Comparison of numerical differential and FFT analyses for evaluating the effect of TMF. (a) Numerical differentiation of the magnetic field. (b) Spectrum analysis of magnetic field by FFT.
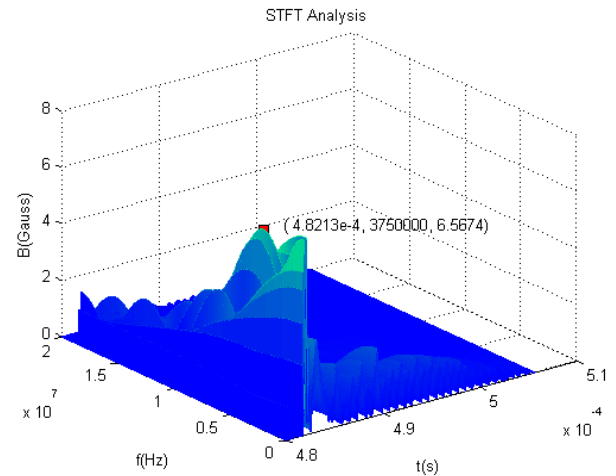

Fig. 10. STFT analysis result of the windowed measured signal. The peak of the signal is denoted as (time, frequency, and magnetic field strength).

generate TMF. The sensor head of this paper is placed close to (<1 cm) the solenoid to measure the TMF. The simulated traveling current [Fig. 7(a)], output current measured by a current probe [Fig. 7(b)], and emanated magnetic field waveform measured by the sensor [Fig. 7(c)] are plotted in Fig 7. It is shown that the proposed TMF measurement system can measure the TMF caused by traveling current wave fairly well.

C. Onsite Testing

To study the performance of the developed system in onsite applications, it was used to measure magnetic fields in various circumstances including power frequency steady state, distorted waveform in reactor, inside High Voltage Direct Current valve house, and switching operations. Fig. 8 shows a typical waveform of TMF for switching operation measured by the developed system. When a switching operation was applied to charge a busbar in the 110-kV substation, the TMF waveform was measured at 3 m directly below the bushing of the transmission line connected to the busbar. The measured

traveling waveform was verified by the similar PSCAD setup as described above. Fig. 9 presents the numerical differentiation and fast Fourier transform (FFT) analysis results of the zoomed-in part of the measured waveform [Fig. 8(d)]. Using FFT method, it can be estimated that the induced voltage is 1.43 V/cm^2 with dominant frequency at 3.66 MHz (with peak magnetic field 6.2183 G), as shown in Fig. 9(b). From the numerical differentiation result [Fig. 9(a)], the evaluated maximum induced voltage is 1.71 V/cm^2. Considering the measurement noise in the signal, these two values can be regarded as almost in the same level. This can be actually further verified by the time frequency analysis. Fig. 10 shows the short time Fourier transform (STFT) analysis of the same window of signal (with Kaiser Window, $N = 7$, $\beta = 0.8$). It is indicated that at 48.213 ms [dB/dt reaches maximum at 48.210 ms, as shown in Fig. 8(a)], there is a maximum component of frequency 3.75 MHz and magnitude 6.5674 G. The corresponding induced voltage is 1.55 V/cm^2. This level of induced voltage may cause significant interference in analog

and digital circuits. Therefore, it is of great application value to have a measurement system that can evaluate the effect of TMF on secondary devices in substations.

IV. CONCLUSION

With the development of the Smart Grid, most functional secondary systems including measurement, communication, and control devices are moving from control rooms to switching yards. This constitutes a great challenge of EMI to these secondary systems when lightning or switching transient occurs. It is necessary to develop a technique that can measure the induced EMI under such conditions. Especially, the effect of EMI on the secondary low-voltage victim circuits must be properly evaluated.

A novel point measurement and evaluation technique for TMF in substations is proposed and a prototype is developed with a broadband MR magnetic sensor. The received disturbance level is defined for evaluating the effect of EMI on victim circuit and the evaluation approach for evaluating the response at any output point is proposed. The effect of sensor size is studied with numerical simulation. The sensor size should be as small as possible in order to enhance the spatial resolution of the TMF measurement. The developed system was tested in both laboratory and field, and the results verify the feasibility and the advantages of the proposed broadband point measurement approach.

Future works will be focused on the extension of the measurement device to broader frequency band, and the field penetration characteristics of different shielding materials under various types of disturbances. In this way, the performance of the shielding of secondary systems in the Smart Grid can be properly characterized, analyzed, and improved.

ACKNOWLEDGMENT

REFERENCES

[1] F. X. Li, W. Qiao, H. B. Sun, H. Wan, J. Wang, Y. Xia, *et al.*, "Smart transmission grid: Vision and framework," *IEEE Trans. Smart Grid*, vol. 1, no. 2, pp. 168–177, Sep. 2010.

[2] M. Camp, H. Garbe, and F. Sabath, "Coupling of transient ultra wide band electro-magnetic fields to complex electronic systems," in *Proc. Int. Symp. Electromag. Compat.*, vol. 2. Aug. 2005, pp. 483–488.

[3] C. M. Wiggins, D. E. Thomas, F. S. Nickel, T. M. Salas, and S. E. Wright, "Transient electromagnetic interference in substations," *IEEE Trans. Power Del.*, vol. 9, no. 4, pp. 1869–1884, Oct. 1994.

[4] Q. Yu and R. J. Johnson, "Smart grid communications equipment: EMI, safety, and environmental compliance testing considerations," *Bell Labs Tech. J.*, vol. 16, no. 3, pp. 109–131, Dec. 2011.

[5] L. D. Grcev and F. E. Menter, "Transient electromagnetic fields near large earthing systems," *IEEE Trans. Magn.*, vol. 32, no. 3, pp. 1525–1528, May 1996.

[6] D. E. Thomas, C. M. Wiggins, F. S. Nickel, C. D. Ko, and S. E. Wright, "Prediction of electromagnetic field and current transient in power transmission and distribution system," *IEEE Trans. Power Del.*, vol. 4, no. 1, pp. 744–754, Jan. 1989.

[7] J. L. Guttman, J. Niple, R. Kavet, and G. B. Johnson, "Measurement instrumentation for transient magnetic fields and currents," in *Proc. IEEE Int. Symp. Electromagn. Compat.*, vol. 1. Aug. 2001, pp. 419–424.

[8] D. Nitsch, M. Camp, F. Sabath, J. Luiken ter Haseborg, and H. Garbe, "Susceptibility of some electronic equipment to HPEM threats," *IEEE Trans. Electromagn. Compat.*, vol. 46, no. 3, pp. 380–389, Aug. 2004.

[9] A. Edelstein, "Advances in magnetometry," *J. Phys., Condensed Matter*, vol. 19, no. 16, pp. 1–28, 2007.

[10] Q. Huang, W. Zhen, and P. W. T. Pong, "A novel approach for fault location of overhead transmission line with noncontact magnetic-field measurement," *IEEE Trans. Power Del.*, vol. 27, no. 3, pp. 1186–1195, Jul. 2012.

[11] M. Vopalensky, A. Platil, and P. Kaspar, "Wattmeter with AMR sensor," *Sens. Actuators A, Phys.*, vols. 123–124, pp. 303–307, Sep. 2005.

[12] A. Baschirotto, E. Dallago, P. Malcovati, M. Marchesi, and G. Venchi, "A fluxgate magnetic sensor: From PCB to micro-integrated technology," *IEEE Trans. Instrum. Meas.*, vol. 56, no. 1, pp. 25–31, Feb. 2007.

[13] A.G. Phadke and J. S. Thorp, *Synchronized Phasor Measurements and Their Applications*. New York, NY, USA: Springer-Verlag, 2008, pp. 1–27.

[14] *Electromagnetic Compatibility (EMC)—Part 4-9: Testing and Measurement Techniques—Pulse Magnetic Field Immunity Test*, IEC Standard 61000-4-9, 2009.

[15] *PSCAD: User's Guide*, Manitoba-HVDC Research Center. Winnipeg, MB, Canada, 2010.